Proceedings of the ASME 2019 Summer Heat Transfer Conference
SHTC 2019
July 15-18, 2019, Bellevue, WA, USA

HT2019-3535

MODIFIED MANIFOLD-MICROCHANNEL HEAT EXCHANGERS FABRICATED BASED ON ADDITIVE MANUFACTURING: EXPERIMENTAL CHARACTERIZATION

William C. Yameen[1], **Nathan A. Piascik**[1], **Andrew K. Miller**[1], **Riccardo C. Clemente**[1]
Jingru Z. Benner[1], **Anthony D. Santamaria**[1], **Seyed A. Niknam**[2], **Mehdi Mortazavi**[1,*]
[1] Department of Mechanical Engineering
[2] Department of Industrial Engineering
Western New England University
Springfield, MA 01119

ABSTRACT

In this study, the additive manufacturing technique has been utilized to fabricate air-water heat exchangers for the application of thermoelectric power plants. Additive manufacturing is a powerful fabrication method that has enabled fabrication of complex geometries that are either challenging or impossible to fabricate based on conventional techniques.Three manifold-microchannel heat exchangers with different interior designs were fabricated by additive manufacturing and from stainless steel. The heat exchangers were tested at different air flow rates and different inlet water temperatures. One heat exchanger was designed and fabricated based on an original design of the manifold-microchannel heat exchanger. Two other heat exchangers were designed with some modifications compared to the original design. In one modified heat exchanger, cylindrical pin arrays were considered on air manifold walls in order to enhance air disturbance, and thus, increase heat transfer between water and air. The second modified heat exchanger contained same pins and also had microchannels in the perpendicular orientation compared to the original design in the outlet manifolds. This design modification was done in order to reduce air-side pressure drop in the heat exchanger. The heat transfer characteristics along with air-side pressure drop were measured and compared with the original design of the manifold-microchannel heat exchanger. Results indicated that the heat flow rate, convection heat transfer coefficient, and pressure drop did not significantly change in modified heat exchangers. For air Reynolds number between around 800 and 4,000, the heat flow rates obtained in the original heat exchanger (type A) and for 50°C water inlet temperature were between 63.9 and 228 W for the lowest and the highest air flow rates, respectively. For the same inlet water temperature, these heat flow rates were between 64.2 and 211 W for the lowest and the highest air flow rates and in one of the modified heat exchangers (type B), respectively. Similarly, while the highest air-side pressure drop in the original heat exchanger was 3458 Pa, this property was measured at 3525 (type B) and 3884 (type C) for the two modified heat exchangers.

NOMENCLATURE

A area [m^2]
c_p specific heat capacity [$kJ/kg \cdot K$]
COP coefficient of performance [-]
f friction factor [-]
h convection heat transfer coefficient [$W/m^2 \cdot K$]
H height [m]
k conduction heat transfer coefficient [$W/m \cdot K$]
L length, thickness [m]
$\dot{m}$ mass flow rate [kg/s]
Nu Nusselt number [-]
P pressure [Pa]
Pr Prandtl number [-]

*Address all correspondence to this author, mehdi.mortazavi@wne.edu

Q heat flow rate [W]
Re Reynolds number [-]
T temperature [°C]
V velocity [m/s]
$\dot{V}$ volumetric flow rate [m^3/s]
W width [m]

Greek Symbols

ρ density [kg/m^3]
μ dynamic viscosity [$N.s/m^2$]

Subscripts

am air manifold
b base
D diameter
fd fully developed
h hydraulic (diameter)
HX heat exchanger
mc microchannel
w water

INTRODUCTION

The condensing system of the power cycle in majority of thermoelectric power plants in the U.S. is based on water cooling. This cooling system in power plants corresponds to 41% of fresh water withdrawal in the U.S. [1]. This significant amount of fresh water withdrawal is costly and adds to the operational cost of the power plant. In addition, this amount of fresh water withdrawal has negative impact on environment. Furthermore, designing power plants based on water-cooled systems dictates specific locations with easy access to fresh water sources. In contrast to water-cooled power plants, air-cooled power plants require little or no water in their cooling systems. However, due to lower specific heat capacity of air compared to water, a larger cooling facility will be required in air-cooled power plants. As a result, only around 1% of the power plants in the U.S. have adopted dry-cooling systems [1]. However, the air-cooled systems can be more appealing to the market if their heat transfer characteristics are enhanced. In addition to an enhanced heat transfer characteristic, the air-side pressure drop should also be reasonable to avoid excess compressing power. All of these requirements can be met in an innovative heat exchanger design. Because the conventional fabrication techniques are limited in capabilities additive manufacturing can be utilized for fabricating more complex heat exchanger designs. Additive manufacturing is a powerful fabrication method that has enabled fabrication of complex geometries that are either challenging or impossible to fabricate based on conventional techniques. Over the last decade, additive manufacturing has developed significantly mainly because of their potential to revolutionize fabrication techniques. Recently, additive manufacturing has been adopted in a wide range of applications such as medical, automotive, aerospace, and construction [2–4]. This is because the additive manufacturing technology has demonstrated great potential for improving materials efficiency, reducing life-cycle impacts, and enabling greater engineering functionality compared to conventional manufacturing [2].

Additive manufacturing also has been utilized in fabricating heat exchangers [5–8] as well as pin fins [9–12]. Kirsch and Thole [12] used laser powder bed fusion (LPBF) methods to fabricate pin fins that can endure in gas turbine engines. They examined the performance of pin fin arrays produced by direct metal laser sintering (DMLS) and observed that the friction factor was extremely high in pin fins fabricated by LPBF compared to other additive manufacturing techniques reported in literature with a marginal benefit in heat transfer. In a similar study, Frester et al. [10] evaluated the heat transfer performance of pin fins fabricated by additive manufacturing and for the application of gas turbine blade cooling. They manufactured triangular, star, and spherical shaped pins based on DMLS and experimentally investigated pressure drop and heat transfer over a range of Reynolds numbers. Parameters they studied included pin fin spacing, number of pin fins, and pin fin geometry. They reported that the additively manufactured triangle and cylinder pin fins outperform conventional pin fin arrays.

In this study, heat transfer characteristics of metallic air-water heat exchangers fabricated via additive manufacturing is investigated. Three heat exchangers were fabricated based on DMLS technology and from stainless steel in EOS M 290. The overall dimensions of heat exchangers are 64.2 $\times$ 46.0 $\times$ 27.1 mm which were designed based on manifold-microchannel heat exchanger concept that had been introduced by Harpole and Eninger in 1991 [13]. In this type of heat exchangers, air is supplied into inlet manifolds from one side and exits the heat exchanger from outlet manifolds on the other side. Each air inlet manifold is blocked at the other side while adjacent manifolds are open at the end side. Air passes from microchannels, fabricated on the top and bottom surfaces of the manifolds, to enter into adjacent manifolds. Water is supplied into water channels located underneath air microchannels. This concept of heat exchanger is schematically shown in Figure 1. In this study the three heat exchangers are referred to as type A, type B, and C. Type A is the original heat exchanger design with no pins on air manifold walls. Type B is similar to type A but includes cylindrical pins on air manifold walls. Type C is similar to type B but has microchannels with different orientation. In outlet air manifolds of the heat exchanger type C, the microchannels are along the direction of air.

The fabricated heat exchangers are shown in Figure 2. While the overall dimensions are identical, the interior design is different between three heat exchangers. In this study, the heat transfer characteristic of heat exchangers is investigated. This study will be followed with a cost analysis study in future. Table 1 lists key dimensions of heat exchangers investigated in this study.

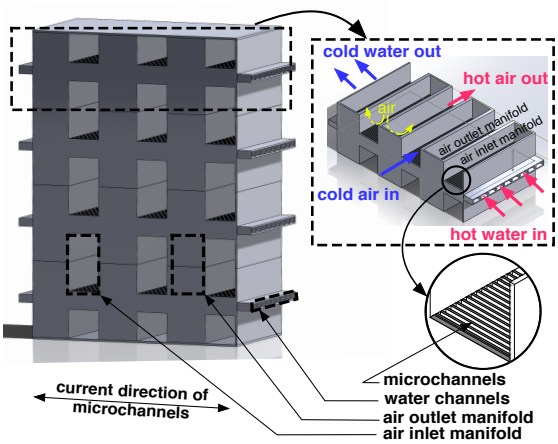

FIGURE 1: SCHEMATIC OF A MANIFOLD-MICROCHANNEL HEAT EXCHANGER

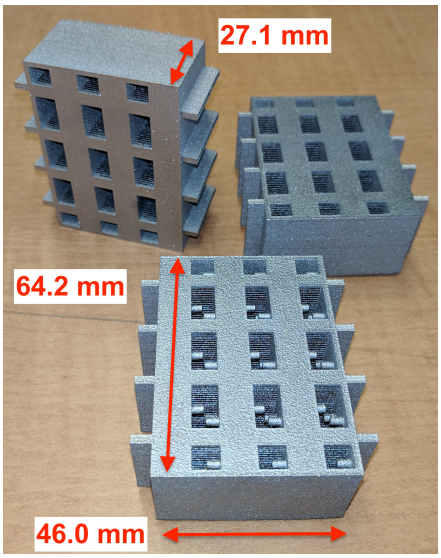

FIGURE 2: ADDITIVELY MANUFACTURED MANIFOLD-MICROCHANNEL HEAT EXCHANGERS FROM STAINLESS STEEL

TABLE 1: HEAT EXCHANGER DIMENSIONS. SOME PROPERTIES ARE SHOWN IN FIGURE 3d.

water channel width	2.60 mm
water channel height	1.10 mm
air manifold width (W_{am})	6.42 mm
air manifold height (H_{am})	11.24 mm
microchannel fin height (H_{mc})	1.0 mm
microchannel width (W_{mc})	0.48 mm
thickness of microchannel fins	0.48 mm
base thickness (L)	0.48 mm
number of water channel rows	4
number of water channel in each row	8
HX overall height (H_{HX})	64.20 mm
HX overall width (W_{HX})	46.02 mm
HX overall depth (D_{HX})	27.16 mm
Thickness of the heat-exchanger body (T_{HX})	1.5 mm
Heat exchanger type A	no pin array (original)
Heat exchanger type B	with pin array
Heat exchanger type C	with pin array and modified microchannel orientation

EXPERIMENTAL SETUP

The experimental setup is schematically shown in Figure 3a. The setup includes a variable speed blower (Republic, HRC 200), a variable frequency drive (VFD), heating bath circulator (Thermo Scientific, S13), rotameter (King Instrument, 7510), and data acquisition system (DAQ). Air, at different flow rates, was supplied into the heat exchanger through a 4" PVC pipe and in an open loop. The rotameter had a measurement range between 6 and 60 scfm, equivalent to 2.83 and 28.3 ℓ/s, respectively. The air pressure drop through the heat exchanger was measured with a pressure transducer with 0 to 6,350 Pa pressure measurement range (Dwyer 668D-08-1). A combination of thermocouples (type T) and RTDs were used to measure the temperature of air and water in inlet and outlet of the heat exchanger. The four temperature measurements were water inlet temperature, water outlet temperature, air inlet temperature, and air outlet temperature. The additively manufactured heat exchanger was inserted in a housing which was also additively manufactured from a photopolymer (RGD720) by Objet, Eden 500V. Experiments were conducted at constant water flow rate and at two different water inlet temperature of 50 and 60°C. All experiments were conducted at room temperature. Figure 3b shows; (1) heating bath circulator, (2) blower, (3) VFD, (4) rotameter, (5) pres-

sure transducer, (6) temperature DAQ board, (7) pressure DAQ board, (8) water flow meter, and (9) the additively manufactured heat exchanger. Figure 3d shows the 2D drawing of the heat exchangers. The pins on the air manifold are only considered in heat exchanger types B and C. The purpose of considering these pins was to enhance air disturbance in air manifolds. Each pin is 2 mm in diameter and is 3 mm in length. Pins are in opposite zigzag arrangement in opposite walls. Figure 3e shows the pins on air manifold walls in the heat exchanger type B. Figure 3f is a section of CAD model to show the pin arrangement in zigzag pattern. Pins fins are designed in opposite configurations in each two opposite air manifold walls. Figure 3g shows the orientation of microchannels in the heat exchanger type C. The highlighted microchannels in this figure are along the air flow direction in air outlet manifolds. In order to facilitate air entrance from air inlet manifolds to air outlet manifolds the side microchannels were designed to be shorter in height. The height of the microchannels in type C were 0.5 mm for side microchannels, 0.75 mm for intermediate microchannels, and 1 mm for middle microchannels, as shown in Figure 3g. The uncertainty in water flow rate, air flow rate, temperature measurement, and pressure measurement were 0.0078 ℓ/s, 0.23 ℓ/s, 0.05°C, and 25 Pa, respectively.

DATA REDUCTION

The experiments were conducted at different air flow rates while the water flow rate was kept constant at 0.047 ℓ/s. The performance of the heat exchanger was evaluated based on air-side heat flow rate, Q_{air}, air-side convection heat transfer coefficient $h_{b,air}$, and air-side pressure drop, ΔP_{air}. The air-side convection heat transfer coefficient was obtained by:

$$Q_{air} = \dot{m}_{air} c_{p,air} (T_{air,out} - T_{air,in}) \tag{1}$$

where $\dot{m}_{air}$, $c_{p,air}$, $T_{air,in}$, and $T_{air,out}$ are air mass flow rate, air specific heat, air temperature in the inlet, and air temperature in the outlet of the heat exchanger, respectively. The air-side convection heat transfer coefficient ($h_{b,air}$) was obtained by:

$$h_{b,air} = \frac{Q_{air}}{A_{base} |\overline{T}_{base} - T_{air,in}|} \tag{2}$$

where A_{base} and $\overline{T}_{base}$ are base surface area and base average temperature, respectively. The base surface area is obtained by:

$$A_{base} = (W_{HX} - 2T_{HX}) \times (D_{HX} - 2T_{HX}) \tag{3}$$

The base temperature can be calculated by performing a one dimensional heat transfer analysis based on water and air temperature.

Assuming water is equally distributed between 32 water channels in the heat exchanger, the water flow rate in each channel is 0.00147 ℓ/s with an average velocity of 0.517 m/s. For turbulent flow the Nusselt number can be obtained based on the correlation proposed by Gnielinski [14]:

$$Nu_D = \frac{(f/8)(Re_D - 1000) \times Pr}{1 + 12.7(f/8)^{1/2}(Pr^{2/3} - 1)} \tag{4}$$

where the friction factor, f, can be obtained by [15]:

$$f = (0.790 \times \ln(Re_D) - 1.64)^{-2} \tag{5}$$

Equation 5 is developed for smooth surface condition. In this study, it is assumed that the water channel surface is smooth. However, the water channel surface condition should be properly explored in future studies. The average Nusselt number for the entire water channel is obtained by [16]:

$$\frac{\overline{Nu}_D}{Nu_{D,fd}} = 1 + \frac{C}{(x/D)^m} \tag{6}$$

where $C = 23.99 \times Re^{-0.23}$, $m = -2.08 \times 10^{-6} \times Re + 0.815$, and x is the length of the flow channel.

The obtained Nusselt number can be used to calculate water convection heat transfer coefficient, $\overline{Nu} = h_w D_h / k$. Finally, the base temperature can be obtained by assuming a uniform heat flux along each air manifold:

$$q'' = \frac{T_{base} - T_w}{\frac{1}{h_w} + \frac{L}{k}} \tag{7}$$

RESULTS

The heat flow rate for the three heat exchangers is shown in Figure 4 as a function of air Reynolds number. The air-side Reynolds number was obtained based on the hydraulic diameter of the microchannels:

$$Re_{air} = \frac{\rho_{air} V D_h}{\mu_{air}} \tag{8}$$

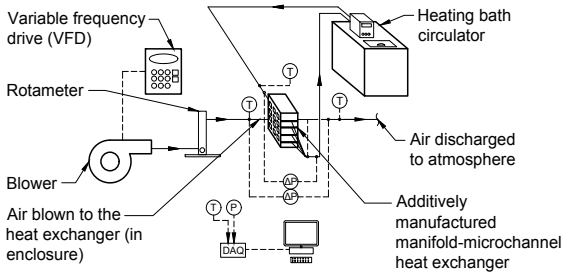

(a)

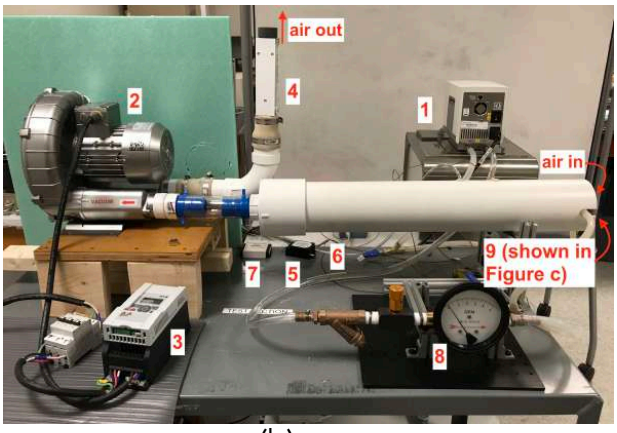

(b)

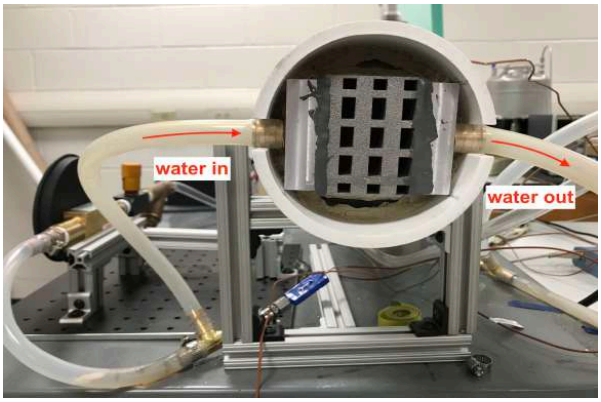

(c)

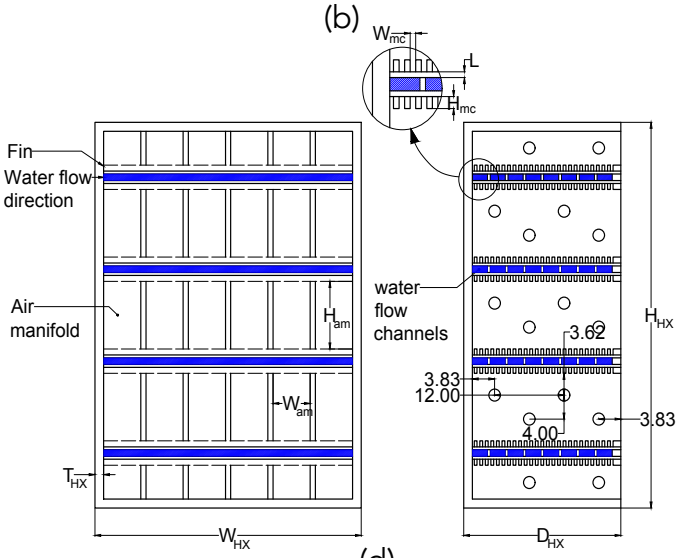

(d)

(e)

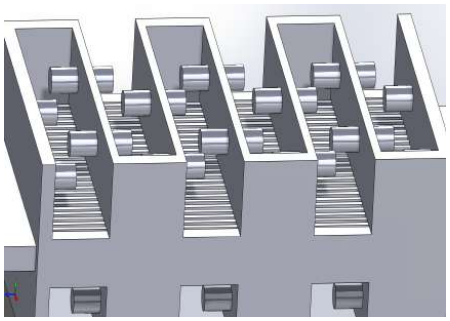

(f)

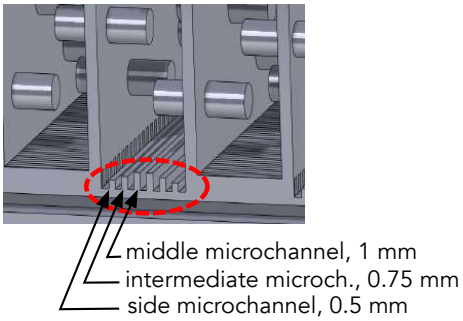

(g)

FIGURE 3: (a) SCHEMATIC OF EXPERIMENTAL SETUP, (b) PHOTO OF THE EXPERIMENTAL SETUP, (c) THE ADDITIVELY MANUFACTURED HX IN A PHOTOPOLYMER HOUSING MANUFACTURED ADDITIVELY, (d) CAD MODEL OF THE HX, (e) PHOTO OF THE FABRICATED HEAT EXCHANGER WITH PINS (TYPE B), (f) SECTION OF CAD MODEL OF PIN CONFIGURATION (TYPE B), (g) MICROCHANNELS ORIENTATION IN HEAT EXCHANGER TYPE C. DIMENSIONS ARE LISTED IN TABLE 1.

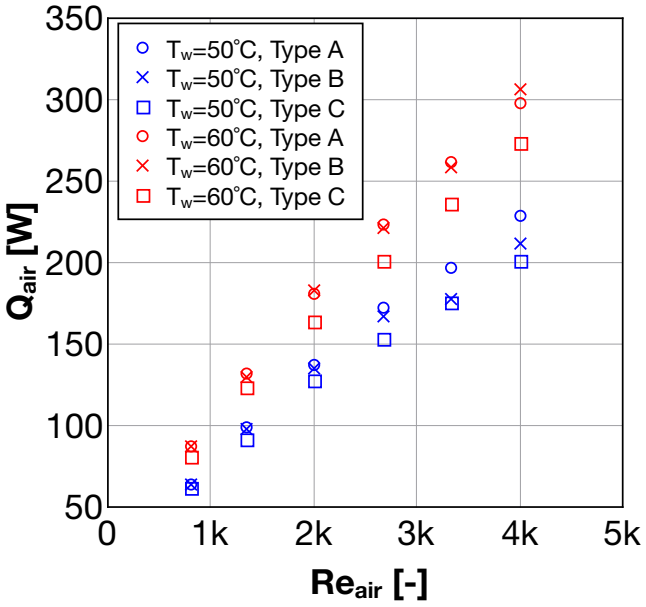

FIGURE 4: COMPARISON OF AIR-SIDE HEAT FLOW RATE.

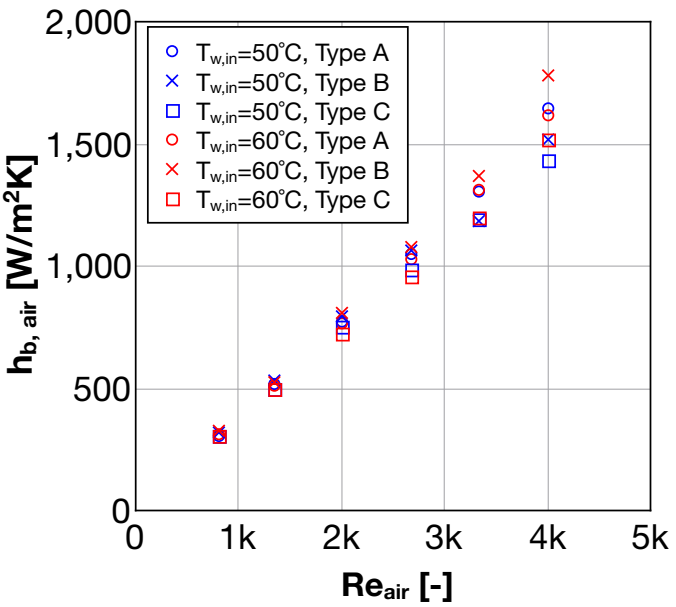

FIGURE 5: COMPARISON OF HEAT TRANSFER COEFFICIENT.

where the hydraulic diameter, D_h, was obtained by:

$$D_h = \frac{4W_{mc}H_{mc}}{2W_{mc} + 2H_{mc}} \tag{9}$$

The general trend observed in this figure suggests that the air-side heat flow rate increases with air Reynolds number. While the calculated heat flow rates are almost identical for lower Reynolds numbers, deviation between air-side heat flow rates for different heat exchangers become more significant for the higher range of air flow rate and for each inlet water temperature. For both water inlet temperature tested in this study, the heat flow rate for heat exchanger type C was the lowest compared to other two heat exchangers. This may be due to the modified air microchannel orientation but further studies should be conducted to confirm this. The highest air-side heat flow rates obtained for 50 and 60°C water inlet temperatures were 228 and 306 W, respectively. Figure 5 shows the air-side convection heat transfer coefficient obtained for three heat exchangers. Similar to heat flow observation discussed in Figure 4, the air-side convection heat transfer coefficient is almost identical for lower Reynolds number. However, some deviations can be observed for higher Reynolds numbers. The highest convection coefficient was calculated at 1777 W/m^2·K for heat exchanger type B and for inlet water temperature of 60°C.

The air-side pressure drop through the heat exchanger is shown in Figure 6. The pressure drop for the range of air flow rate tested in this study was between around 280 and 3,891 Pa for air Reynolds numbers of 800 and 4,010, respectively. These relatively high pressure drops are due to the fact that the inlet air manifolds in this type of heat exchangers are clogged at the end and air is forced to pass through microchannels to enter adjacent manifolds which are open at the exit. The pressure drop data can be used to calculate the air-side coefficient of performance, COP_{air}. The air-side coefficient of performance is obtained by:

$$COP_{air} = \frac{Q_{air}}{\Delta P_{air}\dot{V}_{air}} \tag{10}$$

The air-side coefficient of performance for heat exchanger type A was obtained to be between 4.6 and 109.7. This property for heat exchanger type B was between 4.2 and 103.2 and for heat exchanger type C was between 3.6 and 90.4.

Numerical Simulation

Model Setup A numerical model was built based on the geometry of the heat exchanger shown in Figure 7. The middle section of the heat exchanger is selected as the computational domain (shown in figure below) due to the symmetry in the heat exchanger design. Only the air manifold and the microchannels are considered in the model. Heat generated from the water channels are applied as a constant heat flux boundary condition in the model. The non-uniform temperature distribution will be taken

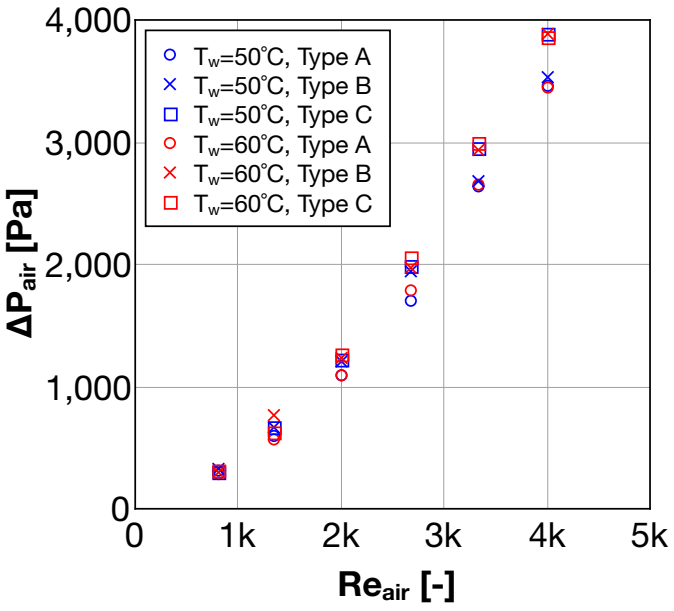

FIGURE 6: COMPARISON OF AIR-SIDE PRESSURE DROP.

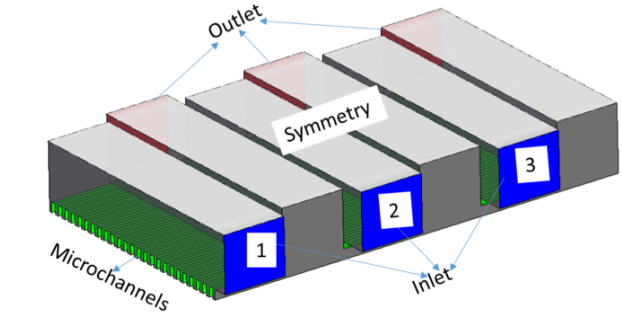

FIGURE 7: COMPUTATIONAL DOMAIN AND BOUNDARY CONDITIONS

in to consideration in future study by adding the liquid channels on the bottom of the microchannel in the model. Three inlets are labeled in Figure 7 and will be referred to accordingly in this section.

The boundary conditions of the model are based on the measurements obtained from the experiments presented in the previous section. The inlet velocity is set at 16.35 m/s, which is based on the highest air flow rate considered in this study (Re=∼4,270). The outlet is set as pressure outlet. A heat flux of 1,240.1 W/m^2 is applied at the bottom of the microchannels. The inlet temperature of the manifold is set at 33.4°C. Due to the design of the heat exchanger, the flow from the inlet manifolds enters the outlet manifolds through multiple microchannels, which alters the flow

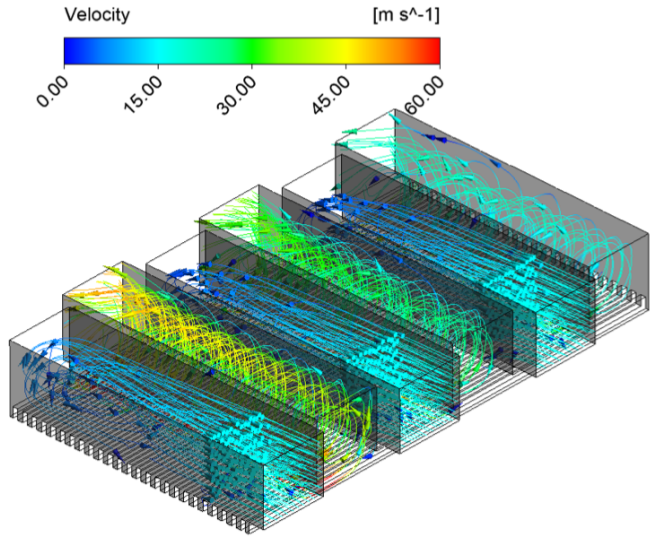

FIGURE 8: STREAMLINES COLORED BY VELOCITY MAGNITUDE

direction and leads to mixing. Therefore, a Reynolds Averaged Navier-Stokes equations (RANS) turbulence model Realizable k-ε model is used to solve the flow field. Commercial Computational Fluid Dynamics (CFD) software ANSYS Fluent 18.1 is used to solve the Navier Stokes Equation. SIMPLE numerical scheme is used, with Standard numerical scheme for pressure interpolation. QUICK scheme is used for momentum and energy discretization, and second order upwind is used for turbulent kinetic energy and dissipation rate discretization. Preliminary results from the model are presented and discussed.

The flow field obtained from the model is shown in Figure 8. Air enters the three individual manifolds as relatively uniform speed, and starts to change direction and flow through the microchannel and towards the outlet. The flow is not symmetrical along the vertical center as flow from inlet 2 and 3 is distributed towards two adjacent outlet manifolds, whereas flow from inlet 1 can only go towards one outlet manifold. Higher flow rate from inlet 1 through the microchannels also leads to the highest local velocity at 78.78m/s. It is worth pointing out that the streamline in Figure 8 shows a noticeable swirling pattern in the outlet manifolds.

The in-plane velocity vector plotted in Figure 9a shows that the flow generates clockwise rotating transverse vortices in the outlet manifolds. A negative pressure zone is formed in the middle of the outlet manifolds due to the transverse vortices shown in Figure 9a. A cross section along the streamwise direction at the outlet adjacent to inlet 1 is shown in Figure 9b. The slice is taken at the outlet manifold next to inlet 1. It shows that the negative pressure zone at the center expands as it gets closer to the exit. While vortices and flow destabilization enhances heat transfer in a lot of cases, transverse vortices could lead to local flow recir-

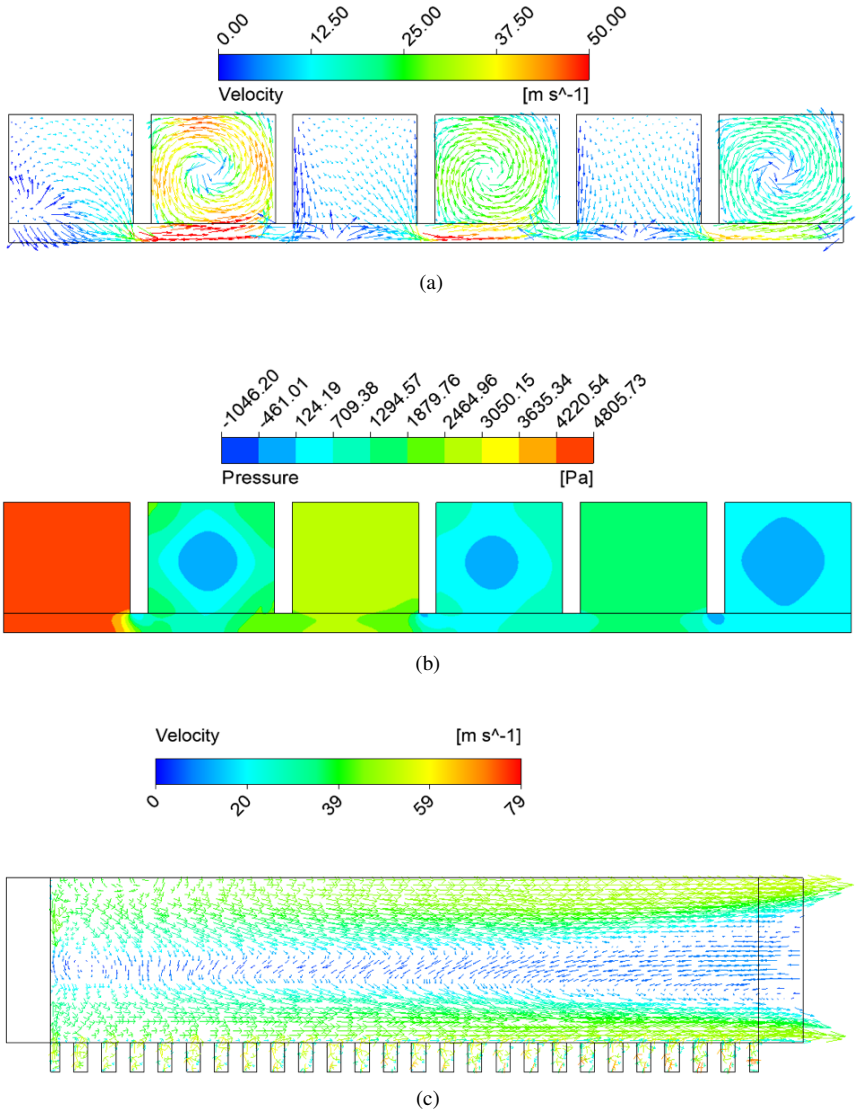

FIGURE 9: (a) VELOCITY VECTOR AT X=12.2 mm, (B) PRESSURE CONTOUR AT X = 12.2 mm, (C) VELOCITY VECTORS IN THE LONGITUDINAL DIRECTION IN THE OUTLET MANIFOLD (Z = 32.8 mm)

culation and reverse flow. The flow pattern shown in the model presents an opportunity for further design modification to improve the performance of the current heat exchanger.

CONCLUSION

The heat transfer characteristic of additively manufactured manifold-microchannel heat exchangers was experimentally evaluated. The heat exchangers were fabricated from stainless steel and by DMLS technology. Air was supplied at different flow rates, ranging between 0.169 and 0.849 m^3/min and water was supplied at a constant flow rate of 0.047 ℓ/s. Separate experiments were conducted for inlet water temperatures of 50 and 60°C. The air-side convection heat transfer coefficient, $h_{b,air}$, air-side heat flow rate, Q_{air}, and air-side pressure drop were obtained in this study. Finally, the air-side coefficient of performance was calculated based on the heat flow rate, air pressure drop, and air flow rate through the heat exchanger. This study showed that additive manufacturing technology can be utilized to fabricate metallic heat exchangers with complex interior designs. However, it was observed that adding pins on air manifolds and/or modifying the microchannel orientation do not impact the heat

transfer and pressure drop properties significantly. For instance, it was observed that heat transfer characteristics between heat exchangers types B and C were almost identical. Similarly, rotating the air microchannels along the direction of air flow in manifolds did not improve the air-side pressure drop in heat exchanger type C. This study is still undergoing by testing heat transfer characteristics for a wider range of air and water flow rates.

ACKNOWLEDGMENT

This study was part of *ME 440 - Senior Design Project* completed by the first four authors as a requirement for their BS degree in Mechanical Engineering at the Western New England University (WNE). Western New England University is gratefully acknowledged for providing the financial support to complete this study. The authors also would like to thank Dave Follette from Advanced Digital Design and Fabrication (ADDFab) [17] at the University of Massachusetts, Amherst for additively manufacturing the heat exchanger.

REFERENCES

[1] S. Acharya, S. Bushart, J. Shi, NSF/EPRI Joint Solicitation Informational Webcast, EPRI and NSF, 2013.

[2] R. Huang, M. Riddle, D. Graziano, J. Warren, S. Das, S. Nimbalkar, J. Cresko, E. Masanet, Energy and emissions saving potential of additive manufacturing: the case of lightweight aircraft components, Journal of Cleaner Production 135 (2016) 1559–1570.

[3] USA DOE, Quadrennial Technology Review 2015 Chapter 6, 2015.

[4] H.S. Glenn, C. Mark, and K. Ben, "3D Opportunity in Medical Technology", April 28, 2014.

[5] M. Arie, A. Shooshtari, S. Dessiatoun, M. Ohadi, Performance characterization of an additively manufactured titanium (ti64) heat exchanger for an air-water cooling application, in: ASME 2016 Heat Transfer Summer Conference collocated with the ASME 2016 Fluids Engineering Division Summer Meeting and the ASME 2016 14th International Conference on Nanochannels, Microchannels, and Minichannels, American Society of Mechanical Engineers, 2016, pp. V002T22A002–V002T22A002.

[6] M. A. Arie, A. H. Shooshtari, R. Tiwari, S. V. Dessiatoun, M. M. Ohadi, J. M. Pearce, Experimental characterization of heat transfer in an additively manufactured polymer heat exchanger, Applied Thermal Engineering 113 (2017) 575–584.

[7] M. A. Arie, A. H. Shooshtari, M. M. Ohadi, Experimental characterization of an additively manufactured heat exchanger for dry cooling of power plants, Applied Thermal Engineering 129 (2018) 187–198.

[8] M. A. Arie, A. H. Shooshtari, V. V. Rao, S. V. Dessiatoun, M. M. Ohadi, Air-side heat transfer enhancement utilizing design optimization and an additive manufacturing technique, Journal of Heat Transfer 139 (3) (2017) 031901.

[9] Y. Cormier, P. Dupuis, A. Farjam, A. Corbeil, B. Jodoin, Additive manufacturing of pyramidal pin fins: Height and fin density effects under forced convection, International Journal of Heat and Mass Transfer 75 (2014) 235–244.

[10] K. K. Ferster, K. L. Kirsch, K. A. Thole, Effects of geometry, spacing, and number of pin fins in additively manufactured microchannel pin fin arrays, Journal of Turbomachinery 140 (1) (2018) 011007.

[11] M. Wong, I. Owen, C. Sutcliffe, A. Puri, Convective heat transfer and pressure losses across novel heat sinks fabricated by selective laser melting, International Journal of Heat and Mass Transfer 52 (1-2) (2009) 281–288.

[12] K. L. Kirsch, K. A. Thole, Pressure loss and heat transfer performance for additively and conventionally manufactured pin fin arrays, International Journal of Heat and Mass Transfer 108 (2017) 2502–2513.

[13] G. M. Harpole, J. E. Eninger, Micro-channel heat exchanger optimization, in: Semiconductor Thermal Measurement and Management Symposium, 1991. SEMI-THERM VII. Proceedings., Seventh Annual IEEE, IEEE, 1991, pp. 59–63.

[14] V. Gnielinski, New equations for heat and mass transfer in turbulent pipe and channel flow, Int. Chem. Eng. 16 (2) (1976) 359–368.

[15] B. Petukhov, T. F. Irvine, J. P. Hartnett, Advances in heat transfer, eds 6.

[16] M. Molki, E. Sparrow, An empirical correlation for the average heat transfer coefficient in circular tubes, Journal of heat transfer 108 (2) (1986) 482–484.

[17] AddFab, UMass Amherst.
URL `https://www.umass.edu/ials/addfab`